Article:
Chen, X., Swift, H.C., Hole, P. et al. (2026) The impact on image formation of inevitable tip bending with modern high resolution atomic force microscopy probes. Nanoscale. ISSN: 2040-3364

https://doi.org/10.1039/d5nr02107c

Nanoscale

PAPER

View Article Online
View Journal

Cite this: DOI: 10.1039/d5nr02107c

The impact on image formation of inevitable tip bending with modern high resolution atomic force microscopy probes

Xinyue Chen, *†[a] Harrison C. Swift,[a] Patrick Hole,[b] Andrew D. L. Humphris[b] and Jamie K. Hobbs *[a]

The majority of atomic force microscopy (AFM) applications rely on tracking and analysing the cantilever motion while assuming the tip is a solid attachment. This assumption is insufficient for accurate imaging with very high aspect ratio (>10 : 1) probes, where tip bending, in addition to cantilever deflection, can significantly distort the morphological image. Here, using quantitative imaging on reference nanostructures and experimental calibration of the tip stiffness, we show that tip bending plays an important role for a range of tested popular commercial AFM probes, even those with relatively low tip aspect ratio, and results in greater than 10 nm errors in measured sample topography in the presence of sufficient tip–sample interaction forces. These effects can be significantly altered by changing the imaging environment. We propose that tip bending should be properly considered in all AFM applications and included in image analysis pipelines to ensure accurate topographic characterisation.

Received 19th May 2025,
Accepted 2nd January 2026

DOI: 10.1039/d5nr02107c

rsc.li/nanoscale

Introduction

Over the last decades, atomic force microscopy (AFM) has been widely applied for investigations across many different research fields. It is a powerful tool to characterise the nanoscale topography, mechanical properties and electrical/electrochemical features of surfaces. The majority of AFM applications rely on a sharp probe that is brought close to and interacts with the sample surface. In addition to a proper selection of AFM probes, including both the cantilever and the tip properties, the performance of AFM measurements is directly limited by the tip parameters. Therefore, tip effects have been widely discussed from many aspects, such as convolution,[1–3] wear and breakage[4,5] and even the relative position of the tip on the cantilever.[6] Researchers have also put considerable effort into designing and manufacturing new types of tips for more challenging applications including improving the imaging resolution[7] and enhancing the ability to quantify three dimensional structures.[8–11]

Most of the discussions regarding the tip effect in AFM applications assumed the tip is a solid, undeformable attachment to the cantilever.[12,13] However, this was proved to be insufficient in studies of critical dimension AFM (CD-AFM), where probes with very high aspect ratio tips (>10 : 1) were often employed to examine the accurate metrology of semiconductor devices at nanometre scales. Benefitting from the regular structure of the sample and a "Step-In" scanning method, the tip motion could be well tracked and it was suggested that such high aspect ratio tips could bend significantly during the imaging process, due to attractive interactions and slippage between the tip and the sample.[14,15] Such tip bending significantly distorted the resultant morphological profiles if no proper corrections were applied.[16] Methods of correcting the tip bending effect from the morphological profile have been discussed and could deliver satisfactory results for imaging regularly nano-structured surfaces.[17,18]

The discussion of such bending effects is so far only prevalent for high aspect ratio tips, because they are more obviously susceptible to bending due to their slender geometries. However, it is important to note that tip bending can occur in other popularly used commercial probes. Many modern AFM probes are designed with extremely sharp tips to achieve high spatial resolution, but this slender geometry also makes the tip susceptible to bending, which has been largely overlooked in most analyses and data interpretation. These sharp probes are used in a broad range of applications, particularly for imaging steep or highly textured surfaces such as nanoparticles, nanopillars and other structures with abrupt height variations. In such cases, the abrupt change in morphology is likely inducing significant tip bending, affecting both imaging accuracy and quantification. Despite this, the mechanical behaviour of the tip itself has received remarkably little atten-

[a]School of Mathematical and Physical Sciences, University of Sheffield, UK. E-mail: jamie.hobbs@sheffield.ac.uk, xinyue.chen@sheffield.ac.uk
[b]Infinitesima Ltd, Abingdon, UK
† Present address: The Henry Royce Institute and School of Chemical, Materials and Biological Engineering, University of Sheffield, UK.

tion to date. In this study, we have not only demonstrated that this concern regarding non-high aspect ratio probes is justified, but also proposed initial strategies to minimise its impact in routine AFM practice. We first measured a reference semiconductor surface with regular periodic nano-trenches to quantitatively illustrate the significant influence of tip bending in the resultant morphological profiles. In addition, the tip stiffness of different types of probes, including both high aspect ratio and widely used non-high aspect ratio ones, were experimentally calibrated. The results showed that the stiffness at the end of a non-high aspect ratio tip can be comparable to that of a high aspect ratio tip, suggesting that both can experience a similar degree of bending during imaging. In this work, we also explored approaches to reduce the tip–sample interactions responsible for such tip bending, including controlling the imaging trigger force and performing measurements in liquid to lower tip–sample forces. These findings lay the groundwork for more in-depth investigations into strategies to mitigate these tip-bending effects in the future.

Materials and methods

Line profile scan and data analysis method on nano-trenches

The CS100 surface, a semiconductor surface featuring periodic nano-trenches of approximately 100 nm in depth and 60 nm in width (Fig. 1a and b), was used as the reference sample to study the AFM probe motion during imaging. Small pieces of CS100 were cleaned by blowing nitrogen over it and then immobilised on a glass slide using a small amount of ReproRubber Thin Pour (Flexbar, USA) for AFM scans.

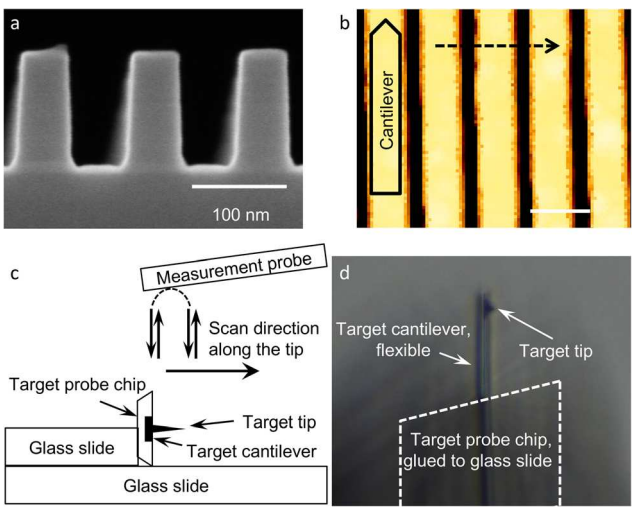

Fig. 1 The standard nano-trench sample (CS100) and illustration of experimental methods. (a) SEM image of a cross-section of CS100. (b) Example topographical image of CS100, obtained using Quantitative Imaging (QI) mode AFM. The cantilever was oriented parallel to the nano-trench direction. The fast scan axis was perpendicular to the trench direction, as indicated by the dashed arrow. Colour scale 0 to 100 nm. Scale bar: 100 nm. (c) Schematic of the experimental setup used to measure the cantilever torsion together with tip bending of various AFM probes. (d) An exemplar optical image of a Biotool High-Resolution probe immobilised as depicted in the schematic.

AFM measurements were conducted on a Nanowizard ULTRA Speed system (JPK, Germany) at room temperature. Two types of AFM probes were employed in line profile scans of this study: Biotool High-Resolution (Nanotools, USA) and AC40 (Bruker, USA). Both probes feature rectangular cantilevers with a nominal spring constant of 0.1 N m^{-1}. The Biotool probe is equipped with a high-aspect ratio (>10 : 1) EBD tip having a radius of 2 nm, while the AC40 probe has a standard sharp silicon tip with a radius of 8 nm. The simple and symmetrical conical geometry of both probe tips enables easier calibration and quantification. Prior to each experiment, the spring constant of each cantilever was determined in air using the integrated contact-free method based on the thermal noise spectrum of vertical deflections.[19] The cantilever deflection sensitivity was acquired under ambient conditions using the same method with the calibrated spring constant. In addition, the lateral deflection spectra were also recorded (1 min) for further calibration of the lateral sensitivity.[20]

Line profiles (length = 100 nm, resolution 0.1 to 1 nm per pixel) were obtained from nano-trenches that were randomly selected based on the surface structure obtained from survey mapping (Fig. 1b). Quantitative Imaging (QI) mode was used throughout, giving a complete force curve (both vertical deflection and lateral deflection *vs.* z displacement) in each pixel of the line profile. The z length of each force curve was set as 400 nm, with an approach speed of 10 μm s^{-1}. Scans over the same line were conducted at different fixed trigger forces (*e.g.* 0.5 nN, 2 nN and 10 nN).

Raw data were exported in .txt format using JPK Data Processing and imported into custom MATLAB algorithms (developed in-house by XC) for all subsequent analyses. Data processing scripts are available upon request. Key parameters, including the trigger, contact, and detach heights, as well as the lateral deflection signal at the trigger point, were extracted from the force curves of each pixel and used to generate various line profiles representing the topography of the nano-trenches as well as the interactions between the AFM tip and the trench.

Experimental measurement of the torsion and tip bending of various AFM probes

The experimental setup for measuring tip bending is illustrated in Fig. 1c. The target probes, which were measured, include the Biotool High-Resolution and AC40 used for nano-trench line profile scans, as well as the USC-F0.3-k0.3 (NanoWorld, Switzerland). The chip of the target probe was carefully mounted onto stacked glass slides using ReproRubber Thin Pour. In this configuration, the target tip extends in a direction perpendicular to the AFM z-sensor motion. Due to the finite thickness of the chip, the cantilever remains sufficiently distant from the glass slides after immobilisation *via* the back side of the chip. As a result, the cantilever retains its mechanical compliance, and the measured

stiffness reflects combined contributions from both cantilever torsion and tip bending.

A tipless MLCT-O10-F probe (nominal spring constant 0.6 N m^{-1}, Bruker, USA) was employed as the measurement probe. A customized ring-shaped probe holder was used in place of the commercial JPK glass holder to prevent the chip of the target probe from crashing into the holder. The target tip was easily located with the aid of the *in situ* optical image (Fig. 1d). The measurement probe was positioned at the target tip, and a low-resolution survey QI image was initially acquired to accurately identify the target tip location. Subsequently, a 1 μm line scan (1 nm per pixel) was performed along the distal end of the target tip (Fig. 1c) in QI mode with a trigger force of 2 nN. Each force curve had a *z*-range of 3 μm and was recorded with an approach speed of 100 μm s^{-1}.

Data were analysed using JPK Data Processing software. The Height Measured channel was offset and used to represent the morphological profile of the target tip. The slope of the final 10 nm indentation of each force–distance curve was extracted to determine the measured stiffness. The spring constant of the measurement probe was calibrated in air using the integrated contact-free method and taken into account in the measured stiffness.

Line profile scan and data analysis method on nano-particles

The polystyrene bead sample was prepared by pipetting 200 μl of 0.045 μm invitrogen carboxylate modified TransFluospheres onto a piece of silicon wafer. The sample was spin coated at 3000 rpm for 1 minute.

The sample was then imaged with the same JPK AFM with AC 40 probes by QI mode. Low-resolution survey mappings were acquired across the sample until a small cluster of beads was identified, allowing a line profile to be obtained over the full length of an individual bead without interference from adjacent beads. Line scans of 120 nm (0.11 nm per pixel) were then taken at a fixed trigger force of 1 nN. Each force curve had a *z*-range of 0.3 μm and an approach speed of 10 μm s^{-1}.

Results and discussion

The AFM probe undergoes a linear motion along the *z*-axis at each imaging pixel in QI mode. This, in turn, facilitates precise monitoring of cantilever deflection both vertically and torsionally (laterally) resulting from interactions with the sample surface (Fig. 2a), which is essential for accurately controlling the trigger forces and estimating the position of cantilever and tip.

Topographic profiles of a 100 nm line over an individual nano-trench (Fig. 2b) were obtained firstly using a commonly used high aspect ratio AFM probe (Biotool High-Resolution) at different trigger force ($F_{trigger}$). The scanning direction was perpendicular to the flexural axis of the cantilever, ensuring that interactions beyond standard repulsion would manifest in lateral deflection rather than vertical deflection, preventing destabilization of trigger forces. The trigger height (*i.e.* piezo displacement with cantilever bending correction corresponding to the trigger force in the approach curve) and the contact point (*i.e.* piezo displacement at the position of significant vertical deflection, measurable relative to the noise, in the approach curve) were read from the vertical force (from vertical cantilever deflection) *vs.* height (*i.e.* piezo displacement in *z*, offset based on the contact position) curves obtained at each

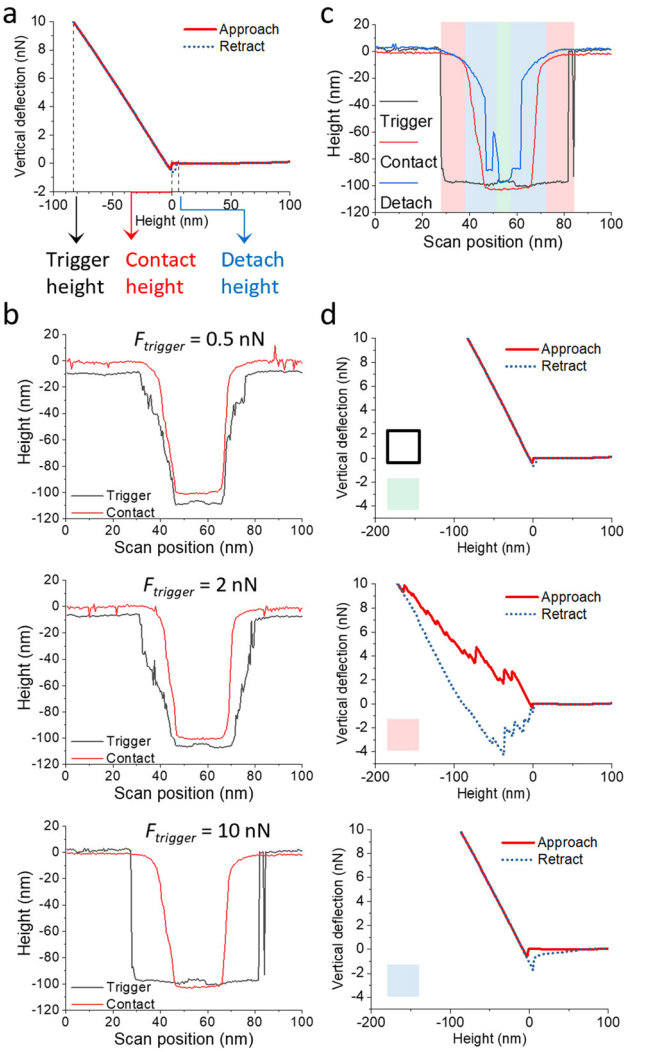

Fig. 2 AFM quantitative imaging of the standard nano-trench (CS100) structure. (a) Example curve of vertical deflection *vs.* height, taken from one pixel in AFM QI imaging. Three height parameters, the trigger height, the contact point and the detach height were read and used to construct alternative topographic profiles of the nano-trench. (b) Topographical profiles from QI scans of a 100 nm line over the same nano-trench, using different trigger force ($F_{trigger}$). Profiles were offset according to the first scanning position (top surface of the nano-trench) of the height determined from the contact (red). Cantilever deflection was subtracted from the height determined from the trigger. (c) Comparison of the topographic profiles over a nano-trench determined from the trigger (black), contact (red) and detach (blue) height. (d) Typical vertical deflection *vs.* height curves obtained from individual approach-retract cycles within different regions along the line scan in (c) (labelled with corresponding background colour).

imaging pixel (Fig. 2a), and used to construct topographic profiles of individual nano-trenches (Fig. 2b). The relative distance between the trigger and contact height profiles is not accurate for several reasons. These include errors in cantilever calibration, torques resulting in excessive flexural and torsional bending of the cantilever, and potentially tip bending that will be discussed later in this work. However, the height change within each profile remains accurate and represents crucial information of the AFM probe motion.

The contact height profiles represent very similar trench structures regardless of the trigger force applied. The stable measured trench depths and sufficient trench widths regardless of trigger force variations indicates the Biotool High-Resolution tip could always visit the narrow trench bottom, benefitting from the high aspect ratio of the tip. The morphological profiles are close to the cross-section of the trench obtained from SEM images, where the slight discrepancy is likely due to the tip convolution (*i.e.* the fact that the tip has a width that is significant compared to the width of the trench). In contrast, the trigger height profiles varied significantly upon changing the trigger force. Significantly larger trench bottom travel lengths were observed in profiles acquired at higher trigger forces. The mean and standard deviation of the measured trench bottom width, summarized from 17 trenches using seven different Biotool HR probes, were 19.0 ± 4.6 nm at 0.5 nN, 23.2 ± 5.0 nm at 2 nN, and 50.7 ± 10.0 nm at 10 nN trigger force. Regardless of the absolute measured values, the trend of increasing trench bottom width with increasing trigger force remained consistent under identical experimental conditions (*i.e.*, when the same probe measured the same line profile). The side wall shape also transitioned to a steep jump at the highest trigger used in this study. Unlike the gradual transition observed at the trench top edges in the contact profile, which more closely reflects the actual shape seen in SEM images, the top trench edges in the trigger profile exhibited a much sharper turn, and even large oscillations over a small region (see the right side of the trigger profile obtained at 10 nN). It is also notable that the trench bottom profile in trigger height is not flat but with a lifted plateau in the central area. The significant divergence of the different height profiles obtained at trigger and contact points illustrates that the AFM tip was not simply doing an ideal "Step-In" motion at all positions along the line scan. Given that the default channel representing morphology in QI imaging, or similar imaging modes on other AFM instrument, is typically dictated by the trigger force height, the risk of having artefacts in resultant morphology due to applying an improper trigger (*i.e.* excessive force) is high, while imaging with very low trigger forces is problematic because of issues with false triggering when considering the inevitable signal noise. To address such artefacts, particularly prevalent in high-resolution imaging of small features, a thorough understanding of AFM tip motions across all dimensions during scanning is essential.

The detach height (*i.e.* piezo displacement corresponding to where the vertical deflection vanished in the retract curve) profile was plotted alongside the trigger and contact height profiles (Fig. 2c). Ignoring the errors in offset due to the cantilever bending corrections, all three profiles remain flat when the tip accesses the top surface and narrow centre of the nano-trench (highlighted in white and green). However, regions proximal to the trench edges (highlighted in red) exhibit notable variability in trigger height, particularly evident with large F_{trigger} as in Fig. 2c. Furthermore, the contact and detach height profiles across regions between the edge and the centre of the trench consistently diverge, irrespective of F_{trigger} value (highlighted in blue).

A revisit of deflection *vs.* height curves obtained from distinct regions can aid in elucidating tip motion and subsequently, height profiles (Fig. 2d). The exemplar vertical deflection *vs.* height curves either atop the trench (white region) or within its narrow central area (green region), demonstrated a characteristic hard-surface contact, elucidating the congruence among the three different height profiles within these regions. When the AFM tip remains in the trench but gets closer to the side wall (blue region), a hard-surface contact phenomenon was similarly observed, albeit with a larger adhesion portion during retraction. While this accounts for the disparity between contact and detach height profiles, it does not adequately clarify the trigger height profile. As the tip traverses the trench edges (red region), it no longer interacts with the surface in a manner of clean vertical compression on a hard surface, which caused the distinct difference in trigger force height.

Simultaneous tracking of lateral deflection *vs.* height (Fig. 3a) provides complementary insights into discerning the tip motion across the four types of regions along the scan over the nano-trench. The lateral deflection change due to the tip–sample compression within the white and green zones remains negligible. Therefore, the tip motion can be considered as an ideal vertical "Step-In" (as in the inset schematic). In the red region, significant lateral signal change, corresponding the irregular contact region vertical deflection in Fig. 2d, was found. This indicates a large rotation of the cantilever most likely due to slipping down the steep trench edge (as in the inset schematic). In the blue region, abrupt lateral deflection change was observed in a reversed direction of those found in the neighbouring trench edge region. This suggests that the cantilever rotates due to an attractive interaction with the trench side wall (as in the inset schematic).

Height profiles determined from the lateral deflection curves (Fig. 3b and c) are nearly identical to those determined from vertical deflection (Fig. 2c), indicating the lateral deflection is accompanying the entire vertical compression process. Plotting the maximum lateral deflection alongside the height profiles (Fig. 3d) reveals the correlation between the different regions in height profiles and variations in cantilever torsion (indicated by lateral deflection readings). The lateral deflection profiles indicate that the cantilever torsion within the slipping regions (*i.e.* red region) was enhanced by increasing F_{trigger}, while remaining the same within all other regions. This suggests increasing trigger resulted in more serious tip slippage across the trench edges. Such slippage enhancement may

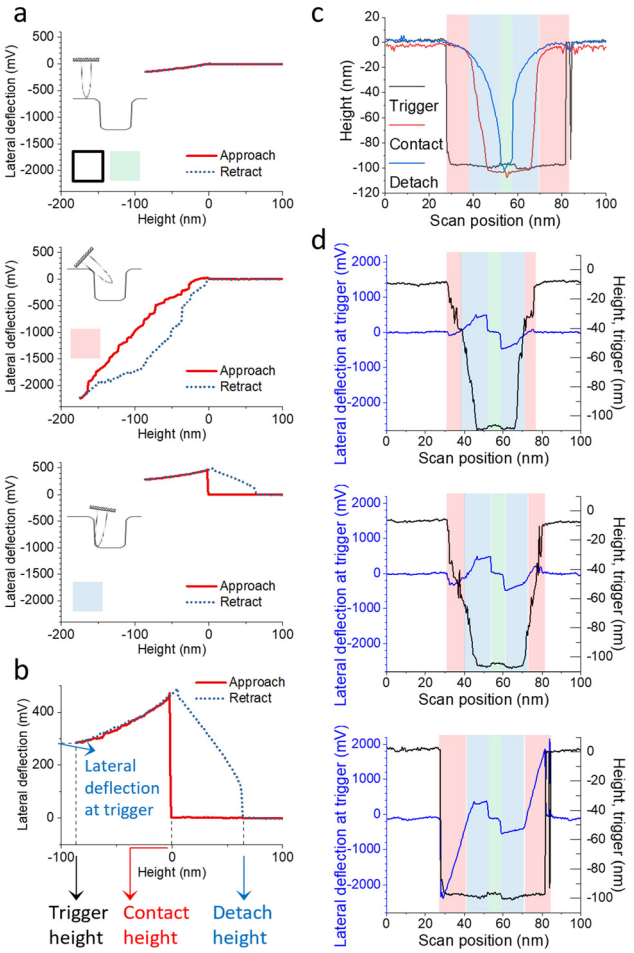

Fig. 3 Lateral motions of the AFM cantilever are correlated with the inconsistency of the topographical profiles determined from different parameters. (a) Typical lateral deflection (*i.e.* torsion) *vs.* height (*i.e.* piezo displacement in *z*, offset based on the contact position) curves obtained simultaneously with the curves in Fig. 2d. (b) Three height parameters, including the trigger, the contact and the detach height that are analogous to those in Fig. 2a, could be read out from each curve and subsequently used to construct different topographical profiles of the nano-trench. In addition, the lateral deflection at the last point of the approach curve (*i.e.* at trigger force point) was extracted to construct the profile of cantilever torsion in imaging. (c) Comparison of the morphological profiles over a nano-trench determined from the trigger (black), contact (red) and detach (blue) height that was extracted from the lateral deflection *vs.* height curves at each scan position, analogous to the profiles determined from the parameters extracted based on vertical deflection data in Fig. 2c. (d) Topographical profiles and the corresponding cantilever lateral deflection at trigger, from QI scans of a 100 nm line over the same nano-trench, using different trigger force ($F_{trigger}$).

exist whenever the AFM tip encounters any steep height change and should be widely considered in AFM imaging. The attraction of the tip by side walls of the nano-trench (*i.e.* blue region), which gives the artefacts in the trench bottom height profiles (*i.e.* the bottom height in this region is lower than the reality), is in contrast not affected by trigger forces. These two cantilever torsional regions are consistent with the phenomenon found from another type of high aspect ratio AFM probe that has a nearly columnar tip shape.[17,18] Quantification of the cantilever torsion can be carried out following calibration, to give accurate information of tip displacement and hence correction of the morphological image.

The torsional sensitivity γ_t can be calibrated using a well-established method based on the thermal noise spectrum.[20,21] For the example Biotool High-Resolution probe used to acquire the data in Fig. 2 and 3, the calibrated γ_t = 2.3 nm V^{-1}. With the lateral deflection profiles in Fig. 3d, the largest tip displacement corresponding to cantilever torsion (*i.e.* assuming the tip is a rigid and undeformable rod) is less than 5 nm at the highest 10 nN trigger. Such tip displacement is not trivial in imaging, yet insufficient to explain the large discrepancy between the trigger height profile and the contact height profile (which we assume approximates the true height). This implies that other motions, which cannot be directly detected from the cantilever bending/torsion, are associated in scanning. For the cantilever, the only other motion, in addition to vertical bending and torsion, will be in-plane bending. As analogous to vertical bending, the spring constant of the in-plane lateral bending k_i can be estimated by classic beam theory,[22] resulting in $k_i \approx 652$ N m^{-1} for the same Biotool High-Resolution probe. The significantly higher spring constant indicates the in-plane lateral bending of the cantilever is negligible. Subsequently, bending of the tip itself is taken into account (Fig. 4a). Previous studies had carefully estimated the tip stiffness of a high aspect ratio columnar shape tip with varying diameters and lengths,[16,17] revealing that tip displacement due to bending can be substantial. Nonetheless, the estimation method lacks accuracy when applied to the cone shaped Biotool High-Resolution probe, as the tip diameter diminishes rapidly towards the tip's end. Another method by Miyazawa *et al.* for estimating the EBD tip stiffness with conical shape[7] gives the tip stiffness at the end k_{tip} = 0.03 N m^{-1} by the following equation:

$$k_{tip} = \frac{\pi E_{tip}}{64}\left\{\int_0^l\int_0^x \frac{l-s}{\left[r_{top}-(r_{top}-r_{end})(s/l)\right]^4}\mathrm{d}s\mathrm{d}x\right\}^{-1}$$

where the end radius of tip r_{end} is assumed as 2 nm and tip radius r_{top} as 10 nm. The Young's modulus of the tip E_{tip} is assumed as 900 GPa. With the same assumption of the tip conditions, finite element analysis gives k_{tip} = 0.53 N m^{-1}. Both estimations suggest that tip stiffness is comparable to the cantilever flexural bending stiffness, which corresponds with substantial tip displacement due to tip bending.

To validate the estimations of tip bending, we experimentally measured the tip stiffness by using a tipless MLCT-O10-F cantilever to perform QI line imaging along the tip from the cantilever side towards the tip end (Fig. 1c). An example of tip stiffness *vs.* distance from the tip end of the Biotool High-Resolution probe is shown in Fig. 4b. The highlighted region (in grey) indicates that the stiffness of the tip dropped dramatically on approaching the tip end. This decrease was not observed in heavily used Biotool probes that likely lack an intact whisker end (*i.e.* unable to properly image

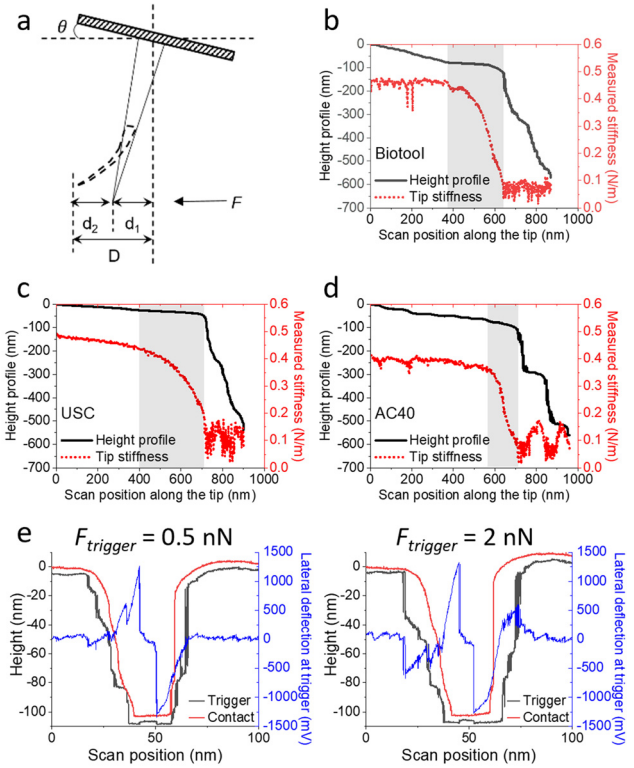

Fig. 4 Tip bending can be significant in AFM probes even without very high aspect ratio tips. (a) Schematic of the tip bending in addition to the cantilever (shaded area) torsion in the presence of a lateral force F at the tip end. It can introduce an additional tip displacement of d_2 due to the tip bending, on top of d_1 that is generated from the cantilever torsion. (b) The morphological (black solid line) and mechanical (red dotted line) profiles of a Biotool High-Resolution probe experimentally calibrated from a line QI scan along the tip (a larger scan position value in x-axis indicates the side closer to the tip end) using a tipless probe (MLCT-O10-F, nominal k = 0.6 N m^{-1}). The same profiles were measured on (c) USC-F0.3-k0.3 (with much lower tip aspect ratio of 5 : 1) and (d) AC40 probes (not high aspect ratio tip). (e) Line scan profiles on the reference CS100 structure, analogous to those in Fig. 1 and 2, using an AC40 probe.

the CS100 sample anymore, data not shown), which further confirms the stiffness drop corresponds to the fine tip. The minimum stiffness, measured at the tip end, is comparable to the vertical spring constant of the cantilever (0.1 N m^{-1}). This is within the range predicted by theoretical methods, and strongly supports the proposal that the AFM tip can be as soft laterally as the cantilever is in the flexural direction. The region with smaller scan position values is closer to the thicker base of the target tip, where the tip behaves increasingly like a solid mass attached to the cantilever. As a result, the stiffness in this area is primarily influenced by the cantilever torsion of the target probe and the nominal spring constant of the measurement probe. Additionally, the profiles did not drop off at the target tip end (*i.e.* the right boundary of the highlighted grey region) but continued, due to the sloped edge of the measurement probe remaining in contact with the target tip.

AFM probes with high aspect ratio tips like the Biotool High-Resolution are frequently employed for specialized tasks like CD-AFM, but less used in the broad range of AFM imaging. A question remains whether comparable levels of tip bending could impact imaging outcomes when employing more widely used commercial AFM probes. Notably, contemporary probes designed for high-resolution imaging often feature extremely small tip radii and "ogee arch" shapes at their ends as a result of manufacturing processes, despite not being classified as high aspect ratio probes. Given the sensitivity of tip stiffness relative to radius, it is reasonable to question whether the tip ends of such non-high aspect ratio probes also exhibit flexibility at the tip end and consequently impact imaging results. We experimentally measure the tip stiffness of two other types of probes, USC-f0.3-k0.3 (tip aspect ratio >5 : 1, NanoWorld) and AC40 (non-high aspect ratio, Bruker) in the same manner as above. The results are shown in Fig. 4c and d. The experimentally measured tip stiffness of all tested AFM probes also showed a dramatic drop getting closer to the fine tip end, which could be as low as the nominal spring constant of the cantilever (*e.g.* ~0.1 N m^{-1}). Therefore, the impact of tip bending is also significant for all the tested probes with lower tip aspect ratio.

The non-high aspect ratio AC40 probe was used to image the reference CS100 structure to compare with the results from Biotool High-Resolution (Fig. 4e). It is clear that the imaging artifacts due to the cantilever torsion and tip bending, as discussed for the results from the high aspect ratio Biotool probes, are still present and significant. To further explore the wider impact of this tip bending effect, we imaged a sample of polystyrene spherical nanoparticles as a proxy for a general nanomaterial (Fig. 5). As the nanoparticles only weakly adhere to the silicon wafer surface, we could not image with high trigger force. However, at relatively low trigger force we see a significant torsional cantilever signal corresponding to the attraction of the tip to the side of the nanoparticle (Fig. 5b), in a similar manner to that seen on the nano-trench sample. On this sample there is not a significant signal due to tip sliding, presumably because of the relatively high adhesive and fric-

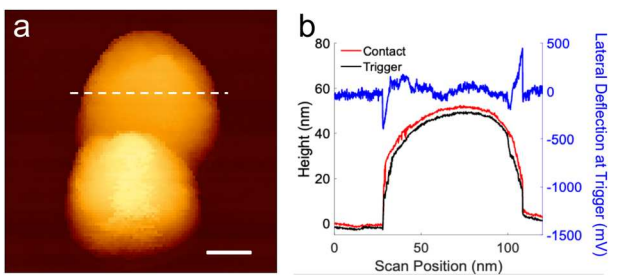

Fig. 5 AFM quantitative imaging of the polystyrene nanoparticles. (a) Example topographical image of nanoparticles. Colour scale 0 to 96 nm. Scale bar: 25 nm. (b) Line profile taken from the location indicated by dashed line in (a). It shows height taken at contact (red) and trigger (black. $F_{trigger}$ = 1 nN), as well as the corresponding lateral deflection at trigger (blue).

tional interaction between the tip and the probe combined with the low maximum trigger force obtainable.

Proper corrections of the cantilever torsion/tip bending can potentially improve the AFM application performance at the analysis stage.[17,18] However, accurate analytical corrections require a quantitatively precise understanding of the tip geometry and tip–sample interactions. In practice, the geometry of the tip and the interaction between the tip and the sample surface can vary considerably. One example is the comparison between Fig. 4e and Fig. 6c, where both profiles were obtained using the same type but different individual probes (both were AC40) and the same trigger settings (0.5 nN) in air, yet they appear significantly different. Furthermore, the imaged structures are often less regular than those presented in exemplar studies across broader AFM applications. These factors make accurate corrections for the effects of the cantilever torsion/tip bending highly challenging in real high-resolution imaging. Exploring a method to mitigate this effect during the experimental stage could be beneficial. In this study, we have presented the resulting profiles obtained using different imaging trigger forces (Fig. 2–4), which clearly indicate that artifacts arising from tip slippage are significantly reduced when a lower trigger force is applied. Therefore, in common imaging, we suggest that the impact due to slippage can be minimised by performing imaging as gently as possible, and by analysing the data to obtain the height at first contact (rather than at the trigger force). However, the impact due to any attractive interactions between the sample surface and the tip, similar to the side wall attraction from the CS100 sample in this study, is not avoidable. In this study, we explored approaches to reduce these interactions during experiments through modification of the environmental conditions. We carried out the same type of experiments in isopropanol (IPA) using both high aspect ratio and non-high aspect ratio probes (Fig. 6). The results clearly indicate the lateral deflection due to side wall attractions robustly vanished, while the lateral deflection due to tip sliding at trench edges was slightly enhanced. These effects arise because the presence of IPA significantly alters the tip–sample interactions. When measurements are performed in IPA rather than in air, capillary forces are largely eliminated due to the removal of adsorbed water layers. The higher dielectric constant of IPA also screens electrostatic and other long-range interactions, such as van der Waals forces, leading to markedly reduced tip–sample adhesion. This reduction explains the disappearance of the lateral deflection peak highlighted by the green arrows in Fig. 6. Moreover, the liquid environment decreases interfacial friction,[2,3] which slightly enhances tip slippage, as evidenced by the deflection peak indicated by the black arrows in Fig. 6. Consequently, the probes were better able to reach the bottom of the narrow trench in IPA compared to air, as evidenced by the wider and cleaner imaged trench bottom profiles (*i.e.* no lateral deflection over a large trench bottom area). The presence of IPA enabled the non-high-aspect-ratio AC40 probe to access the nano-trench more effectively than the high-aspect-ratio Biotool probe in air. This highlights the critical influence of the ambient environment on imaging quality. Accordingly, adjusting ambient conditions to modify the interactions between the tip and the sample surface can serve as an effective approach to minimise undesirable interactions or enhance beneficial ones, thereby improving measurement performance. Indeed, imaging in liquid, as demonstrated in this study, is not a universal solution for improving imaging quality and presents certain practical limitations. In practice, the chosen liquid must be compatible with the sample and should not induce damage or structural changes. Some samples may lose adhesion to the substrate or become unstable in a liquid environment, and complete removal of the liquid after imaging can be difficult. These factors must be carefully considered when evaluating the suitability of liquid-based imaging for a given application.

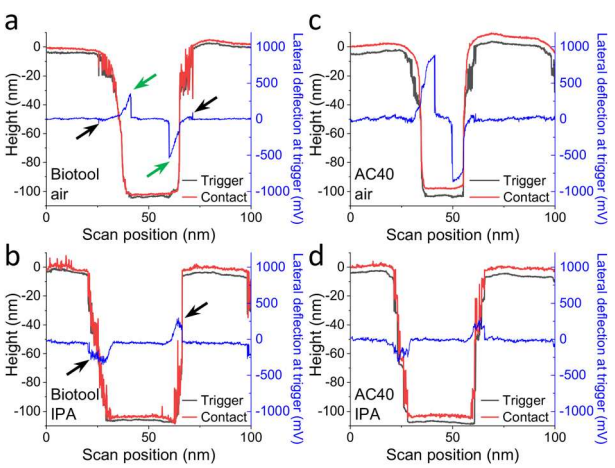

Fig. 6 The impact of imaging environment on tip–sample interactions. The height determined from contact (red), height determined from trigger (black, $F_{trigger}$ = 0.5 nN) and the corresponding lateral deflection at trigger (blue) profiles over a nano-trench on the reference CS100 structure were constructed from QI line scans using either (a and b) Biotool High-Resolution or (c and d) AC40 probes. Measurements were performed in air (a and c) and IPA (b and d). Peaks in the lateral deflection indicated by black arrows correspond to torsional responses induced by tip slippage, whereas those marked by green arrows arise from sample sidewall attraction. The slippage-induced torsion was enhanced in IPA, while the sidewall attraction effects vanished.

Conclusion

In summary, we propose that the cantilever torsion/tip bending can have significant impact on AFM applications, more than that has been recognised so far, and should be taken into account properly for more accurate AFM image quantification. We experimentally determined the tip bending effect, in combination with the cantilever torsion in this study, and revealed this is a common effect for a number of popular modern AFM probes with fine ends, and not only limited to a certain field of AFM application (*e.g.* critical dimensional AFM). This effect must be carefully considered, especially

when measuring relatively stiff samples (*i.e.*, with stiffness exceeding that of the AFM tip) in regions with pronounced topography and steep angles (*e.g.* calibrating the tip geometry using a high-aspect-ratio grid). In particular, when the tip is sharp and the characteristic length scales of the sample roughness are large compared to the tip radius, it is worthwhile considering the possibility of the problems described above arising. Experimentally, examining the lateral deflection channel can help indicate where the problem may exist. We also note that ignoring this effect can compromise quantitative mechanical mapping, for example, by introducing errors in adhesion measurements. Mathematical correction of the discussed effects would require precise knowledge of the tip geometry and tip–sample interactions across experiments, which is extremely challenging in practice. Therefore, we recommend minimising undesired tip–sample interactions during measurements by employing the gentlest possible imaging force and optimising the imaging environment. Our results further demonstrate that the profile obtained at the contact point effectively eliminates most artifacts present in the trigger profile. Consequently, using the contact-point profile provides a more reliable and efficient approach for AFM characterisation and represents a straightforward means to improve measurement accuracy.

Author contributions

XC designed the study, performed the experiments, analysed and interpreted the data, and wrote the manuscript. HCS performed the nanoparticle experiments and analysed the data. PH and ADLH designed the study, interpreted the data and helped write the manuscript. JKH designed the study, interpreted the data, wrote the manuscript and directed the project.

Conflicts of interest

PH and ADLH work for Infinitesima Ltd, a semiconductor metrology company that sells an AFM based surface metrology tool.

Data availability

The authors confirm that the data supporting the findings of this study are available within the article. Raw data are available from the corresponding author upon request.

Acknowledgements

This research was supported by UKRI, grant numbers EP/R511754/1 and EP/W524360/1. For the purpose of open access, the author has applied a Creative Commons Attribution (CC BY) licence to any Author Accepted Manuscript version arising.

References

1 H. Itoh, T. Fujimoto and S. Ichimura, *Rev. Sci. Instrum.*, 2006, **77**, 103704.
2 J. Shen, D. Zhang, F.-H. Zhang and Y. Gan, *Appl. Surf. Sci.*, 2017, **422**, 482–491.
3 J. Canet-Ferrer, E. Coronado, A. Forment-Aliaga and E. Pinilla-Cienfuegos, *Nanotechnology*, 2014, **25**, 395703.
4 T. Strahlendorff, G. Dai, D. Bergmann and R. Tutsch, *Ultramicroscopy*, 2019, **201**, 28–37.
5 J. Liu, J. K. Notbohm, R. W. Carpick and K. T. Turner, *ACS Nano*, 2010, **4**, 3763–3772.
6 F. Mokhtari-Nezhad, A. R. Saidi and S. Ziaei-Rad, *Ultramicroscopy*, 2009, **109**, 1193–1202.
7 K. Miyazawa, H. Izumi, T. Watanabe-Nakayama, H. Asakawa and T. Fukuma, *Nanotechnology*, 2015, **26**, 105707.
8 H. Xie, D. Hussain, F. Yang and L. Sun, *Rev. Sci. Instrum.*, 2014, **85**, 123704.
9 J. Choi, B. C. Park, S. J. Ahn, D.-H. Kim, J. Lyou, R. Dixson, N. Orji, J. Fu and T. Vorburger, *J. Micro/Nanolithogr., MEMS, MOEMS*, 2016, **15**, 034005.
10 R. Zhang, S. Wu, L. Liu, N.-H. Lu, X. Fu, S.-T. Gao and X.-D. Hu, *Meas. Sci. Technol.*, 2018, **29**, 125011.
11 A. Savenko, I. Yildiz, D. H. Petersen, P. Bøggild, M. Bartenwerfer, F. Krohs, M. Oliva and T. Harzendorf, *Nanotechnology*, 2013, **24**, 465701.
12 T.-S. Wu, W.-J. Chang and J.-C. Hsu, *Microelectron. Eng.*, 2004, **71**, 15–20.
13 Y. Song and B. Bhushan, *J. Appl. Phys.*, 2006, **99**, 094911.
14 S. Hosaka, T. Morimoto, H. Kuroda, Y. Minomoto, Y. Kembo and H. Koyabu, *Appl. Surf. Sci.*, 2002, **188**, 467–473.
15 T. Morimoto, H. Kuroda, Y. Minomoto, Y. Nagano, Y. Kembo and S. Hosaka, *Jpn. J. Appl. Phys.*, 2002, **41**, 4238.
16 V. Ukraintsev, N. Orji, T. Vorburger, R. Dixson, J. Fu and R. Silver, *J. Micro/Nanolithogr., MEMS, MOEMS*, 2013, **12**, 023009.
17 M. Watanabe, S. Baba, T. Nakata, T. Morimoto and S. Sekino, *A novel AFM method for sidewall measurement of high-aspect ratio patterns*, SPIE, 2008.
18 M. Watanabe, S. Baba, T. Nakata, T. Morimoto, S. Sekino and H. Itoh, *J. Micro/Nanolithogr., MEMS, MOEMS*, 2012, **11**, 011009.
19 J. L. Hutter and J. Bechhoefer, *Rev. Sci. Instrum.*, 1993, **64**, 1868–1873.
20 N. Mullin and J. K. Hobbs, *Rev. Sci. Instrum.*, 2014, **85**, 113703.
21 C. P. Green, H. Lioe, J. P. Cleveland, R. Proksch, P. Mulvaney and J. E. Sader, *Rev. Sci. Instrum.*, 2004, **75**, 1988–1996.
22 J. E. Sader and C. P. Green, *Rev. Sci. Instrum.*, 2004, **75**, 878–883.
23 F.-C. Hsia, C.-C. Hsu, L. Peng, F. M. Elam, C. Xiao, S. Franklin, D. Bonn and B. Weber, *Phys. Rev. Appl.*, 2022, **17**, 034034.

